



ORIGINAL ARTICLE

Computational modeling of plain and steel fiber-reinforced concrete beams without transverse reinforcement

Modelagem computacional de vigas de concreto simples e reforçadas com fibras de aço sem armadura transversal

Daniel de Lima Araújo^a Cleiton Rodrigues Siqueira Filho^a Fausto Arantes Lobo^a ^aUniversidade Federal de Goiás – UFG, Escola de Engenharia Civil e Ambiental, Goiânia, GO, Brasil

Received 18 September 2022

Accepted 23 March 2023

Abstract: Finite element analysis with nonlinear material behavior modeling can be used to design concrete structures. This study aimed to develop a computational model to represent the shear behavior of concrete beams without transverse reinforcement described in the literature, with or without steel fibers. Two different approaches of finite element analysis were investigated, namely smeared and discrete crack models. The results of the smeared crack model were compared with the results of double-notched push-through tests, and an empirical equation for the shear retention factor of plain concrete was suggested. The computational model using a discrete crack approach with representation of the aggregate interlocking mechanism was compared with the results of push-of test, and an accurate correlation was observed up to the maximum shear stress. It was concluded that the discrete crack approach provided the most accurate representation of the shear behavior of a non-reinforced beam with a shear span-to-depth ratio of 2.17. However, for a non-reinforced beam with a shear span-to-depth ratio of 2.66, the smeared crack approach accurately represents the shear strength and stiffness of the beam. The shear retention factor had little influence on the overall behavior of a steel fiber-reinforced concrete beam. Finally, it was concluded that a variable shear retention factor should be used in the smeared crack approach with fixed crack, as a constant shear retention factor tends to overestimate the shear strength of beams.

Keywords: nonlinear finite element analysis, shear, steel fiber-reinforced concrete, shear retention.

Resumo: O Método dos elementos finitos considerando o comportamento não-linear do material pode ser usado no projeto de estruturas de concreto. Este trabalho teve como objetivo desenvolver um modelo computacional para representar o comportamento ao cisalhamento de vigas de concreto sem armadura transversal descritas na literatura, com ou sem a incorporação de fibras de aço. Duas abordagens diferentes pelo método dos elementos finitos foram investigadas, a saber, modelos com fissuração discreta ou distribuída. Os resultados da modelagem com fissuração distribuída foram comparados com os resultados de ensaios de cisalhamento direto em corpos de prova com duplo entalhe, sendo proposta uma equação empírica para o fator de retenção ao cisalhamento do concreto simples. O modelo computacional usando uma abordagem de fissuração discreta com representação do mecanismo de intertravamento do agregado foi comparado com os resultados de ensaios de cisalhamento direto, tendo sido observada uma boa correlação até a tensão de cisalhamento máxima. Concluiu-se que a melhor representação do comportamento de uma viga de concreto armado sem estribos e com uma relação entre vão cisalhamento e altura de 2,17 foi obtida com a abordagem de fissuração discreta. No entanto, para uma viga sem estribos e com uma relação entre vão de cisalhamento e altura de 2,66, a abordagem de fissuração distribuída representou com precisão a resistência ao cisalhamento e a rigidez da viga. O valor escolhido para o fator de retenção ao cisalhamento teve pouca influência no comportamento de uma viga de concreto reforçado com fibras de aço. Por fim, concluiu-se que na abordagem com fissuração distribuída e fissura fixa deve-se utilizar um fator de retenção ao cisalhamento variável, pois o fator de retenção ao cisalhamento constante tende a superestimar a resistência à força cortante das vigas.

Palavras-chave: análise não linear pelo método dos elementos finitos, cisalhamento, concreto reforçado com fibras de aço, fator de retenção ao cisalhamento.

Corresponding author: Daniel de Lima Araújo. E-mail: dlaraujo@ufg.br

Financial support: This study was financed in part by the Brazilian Federal Agency for Support and Evaluation of Graduate Education (CAPES, Finance Code 001). The authors would also like to thank the Goiás State Research Foundation (FAPEG, grant no. 2017.10.267000.513) and the Brazilian National Council for Scientific and Technological Development (CNPq, grant no. 552118/2011-7) for financing this research.

Conflict of interest: Nothing to declare.

Data Availability: The data that support the findings of this study are available from the corresponding author, D.L. Araújo, upon reasonable request.



This is an Open Access article distributed under the terms of the Creative Commons Attribution License, which permits unrestricted use, distribution, and reproduction in any medium, provided the original work is properly cited.

How to cite: D. L. Araújo, C. R. Siqueira Filho, and F. A. Lobo, "Computational modeling of plain and steel fiber-reinforced concrete beams without transverse reinforcement," *Rev. IBRACON Estrut. Mater.*, vol. 16, no. 3, e16311, 2023, <https://doi.org/10.1590/S1983-41952023000300011>

1 INTRODUCTION

Several parameters have a significant influence on the shear resistance of concrete. In normal-strength concrete, cracking commonly occurs throughout the matrix and in the interface zone between the matrix and coarse aggregate because of the high strength of the latter. High-strength concrete has a different mode of fracture in that cracks develop through coarse aggregate, creating a smoother crack surface. This mechanism is known as aggregate interlock.

Shear transfer along a rough crack depends on aggregate size, crack width, and concrete compressive strength. Aggregate interlock experiments show that the resistance on the crack surface depends not only on tangential crack displacements but also on normal crack displacements and their interaction. This phenomenon is denoted as crack dilatancy.

Deng et al. [1] demonstrated that coarse aggregate size does not directly influence the cracking load of a beam without transverse reinforcement tested in shear. However, the ultimate load of the beam was found to increase with increasing aggregate size, indicating that aggregate size directly influences shear capacity. Sells et al. [2] showed that coarse aggregate size had little impact on shear resistance, but the effect of aggregate type appeared to be highly significant. Compared to limestone aggregate, a material with a weak nature, river gravel improved the shear resistance of reinforced concrete beams.

It is recognized that the use of steel fibers in concrete promotes greater tensile strength, creating a bridging effect on cracks. As a result, aggregate interlock linked to coarse aggregates can be optimized, given that fibers reduce crack width, thereby increasing interlocking between coarse aggregates on the fracture surface [3], [4].

There are several methods for modeling cracking in nonlinear finite element analyses of reinforced concrete, with smeared and discrete approaches being the most common. Araújo et al. [5] suggested that the discrete crack model is preferable for structures with few cracks. The discrete crack approach considers a crack to be a geometric discontinuity in the finite element mesh; therefore, it is necessary to define the direction and position of cracks before proceeding with the analysis. This approach can be used to solve problems involving push-off tests and pre-cracked structures, among others. In this approach, the aggregate interlock phenomenon can be implemented in interface elements by using empirical and analytical formulas that simulate the transfer of shear stresses through cracked concrete planes. Examples of empirical and analytical formulations for aggregate interlock can be found in previous studies [6]–[9].

In the smeared model, a crack is not represented by a single crack but rather by a cracked element area. The finite element mesh does not need to be redefined during the analysis, unlike in the discrete crack approach. The smeared crack concept is suitable for analyses of adequately reinforced structures where cracks are distributed. When the maximum principal stress exceeds the ultimate strength of the material, cracks will appear in the direction perpendicular to the direction of the maximum principal stress at Gauss points of finite elements. Smeared crack models commonly use a total strain-based approach, typically assuming a rotating or fixed crack direction.

As cracks appear in concrete and crack width increases, the ability of the crack surface to transmit shear stresses decreases. In smeared crack models, such a loss is accounted for by a shear retention factor ($0 \leq \beta \leq 1$), which reduces the elastic shear modulus upon cracking of concrete. Slobbe et al. [10] explain that the shear retention factor can be interpreted as a means of modeling aggregate interlock. The relationship between the shear retention factor and the crack shear modulus – a mode II fracture parameter of concrete – can be explained by noting that the reduced shear stiffness is associated with the total strain, while the crack shear modulus is associated with the crack strain.

The assumption of a linear relationship between shear stresses and strains after cracking creates multiple problems. Smeared crack models are extremely sensitive to the shear retention factor, which is either taken as a constant or as a function of current crack normal strain [11]. This is particularly relevant because the β value is often chosen rather arbitrarily. Large values for the β factor can result in stress locking, whereas small values may lead to convergence problems.

Several authors have proposed different values for the shear retention factor. For example, Araújo et al. [5] used a constant β value of 0.01 when modeling the results of direct shear and bending tests of reinforced concrete beams. The same authors used β values of up to 0.5 for steel fiber-reinforced concrete beams. Sagaseta [12] reported that a constant β value of 0.1 or 0.2 is commonly used but noted, however, that, according to experimental evidence, this factor is not constant and decreases as crack width increases. Scotta et al. [13] showed that the adoption of constant β values greater than 0.2 overestimates the strength of concrete beams without stirrups. Furthermore, the authors did not observe any variation in beam resistance with β values above 0.2. Because of this, they recommended that a variable value should

be used for the shear retention factor, with a linear decay rate ranging from 1 to 0. This conclusion agrees with the observations of Hendriks et al. [14], who strongly recommended the adoption of a variable shear retention factor in fixed crack models. Models with constant shear retention are not recommended, because they tend to overestimate the stiffness of beams and slabs. Moreover, for beams and slabs without transverse reinforcement, the adequacy of a variable shear retention factor should be explicitly verified. Alternatively, for beams, shear stiffness could be gradually reduced to zero when the crack width is half the average aggregate size.

Several studies in the literature have proposed expressions for the reduced shear modulus of cracked concrete. These expressions are dependent on the crack normal strain (ε_{nn}) and the stress-free crack normal strain ($\varepsilon_{nn,ult}$). In these studies, the shear retention factor decreases as the crack normal strength increases, which is attributed to the reduction in interlock of aggregate particles as the crack opening increases. When the shear retention factor tends to zero, it indicates that the shear stiffness from aggregate interlock across macro-cracks is being disregarded. This has no significant consequences if the crack normal stress is tensile instead of compressive.

Al-Mahaidi [15] proposed a variable β value that depends on tensile strength (f_t), modulus of elasticity (E), and crack normal total strain (ε_{nn}), according to Equation 1.

$$\beta = 0.4 \frac{f_t}{E \varepsilon_{nn}} \quad (1)$$

Figueiras [16] proposed a linear decay model for the shear retention factor that starts at 0.25 and depends on the crack normal total strain and ultimate normal strain of the element ($\varepsilon_{nn,ult} = 0.0045$). Equation 2 expresses this relationship.

$$\beta = 0.25 \left(1 - \frac{\varepsilon_{nn}}{\varepsilon_{nn,ult}} \right) \quad (2)$$

Rots and Blaauwendraad [17] proposed a similar decay model that depends on the crack normal strain of the element and factor k , which is generally equal to 1, as given by Equation 3.

$$\beta = \left(1 - \frac{\varepsilon_{nn}}{\varepsilon_{nn,ult}} \right)^k \quad (3)$$

Červenka et al. [18] proposed a logarithmic decay model as a function of the crack normal strain and the geometric rate of reinforcement (ρ) that crosses the section, expressed by Equation 4.

$$\beta = \frac{-1}{10-167(\rho-0.005)} \ln \left(\frac{1000\varepsilon_{nn}}{7+333(\rho-0.005)} \right) \quad (4)$$

In the previous equations, the stress-free crack normal strain ($\varepsilon_{nn,ult}$) is not considered a separate material in tension. Instead, it is a result of the crack bandwidth and the properties of the concrete in tension, such as tensile strength, fracture energy, and the chosen softening diagram for concrete.

Although a variable shear retention factor is more adequate to describe shear transfer in fixed cracked models than a constant shear retention factor [17], it has certain limitations in representing shear transfer through a macro-cracked plane. Therefore, studies investigating the most appropriate value for the shear retention factor in finite element modeling of concrete structures are still needed.

2 EXPERIMENTAL PROCEDURES

Tests were carried out to obtain in advance the parameters for the computational modeling of concrete beams without transverse reinforcement subjected to shear failure. Two types of direct shear tests were performed: a double-notched push-through test and a push-off test on a specimen with a pre-cracked shear plane. Details of test procedures are described elsewhere [3].

2.1 Double-notched push-through tests

These tests were conducted on a plain concrete mixture comprising a coarse aggregate with a maximum dimension of 9.5 mm (F-00-1) and 12.5 mm (F-00-2). The mechanical properties of the concrete used in these tests are shown in Table 1. At least three 150 × 150 × 500 mm prismatic specimens were used for each mixture. Prior to the test, 35 mm deep, 5 mm wide notches were cut along the perimeter of the transversal section of the specimens, in the middle third of the span. Therefore, each specimen had two shear crack planes 163 mm from the end, with approximate dimensions of 80 × 80 mm. After the test, the effective dimension of the shear plane was evaluated.

Table 1. Mechanical properties of concrete.

Mixture	v_f (%)	f_{cm} (MPa)		f_{ctm} (MPa)		E_{cm} (GPa)		G_f^I (N/mm)	
		Mean	SD	Mean	SD	Mean	SD	Mean	SD
F-15-2	1.50	68.74	8.57	3.93	1.02	40.39	1.84	5.96	0.97
F-00-2	0.00	65.08	4.73	4.13	0.90	39.04	0.74	0.16	0.01
F-00-1	0.00	66.29	6.54	5.18	-	37.96	1.67	-	-

v_f : volume of steel fibers; f_{cm} : mean value of compressive strength of concrete; f_{ctm} : mean value of axial tensile strength of concrete; E_{cm} : mean value of modulus of elasticity of concrete; G_f^I : fracture energy of concrete.

The specimen was supported by two edges 163 mm apart. Thus, a narrow region of the specimen between the loading and support edges was directly subjected to shear stress. One end was supported by a bearing surface, which provided both horizontal and vertical restraining forces. At the other end, a roller support produced only a vertical restraining force. Additional roller supports were used on the upper face of the specimen where force was applied by the machine. In the original test setup, the shear plane is always accompanied by a normal stress due to loads and reactions acting centrally on the loading plates. Consequently, the shear plane is subject to global bending and arch effect, which compress the upper face of the shear plane and tended to overestimate its shear capacity [3], [19], [20]. However, the test setup used in this study was modified and does not introduce a normal stress on the shear planes due to the roller supports used on the specimen supports and the machine's load cell. Furthermore, specimens were instrumented to measure shear slip and crack dilatancy on both shear planes. The test apparatus is shown in Figure 1.

Displacement was applied to the middle part of the specimen between two shear planes using a non-closed loop machine. The velocity of displacement was set at 0.02 mm/min throughout the test.

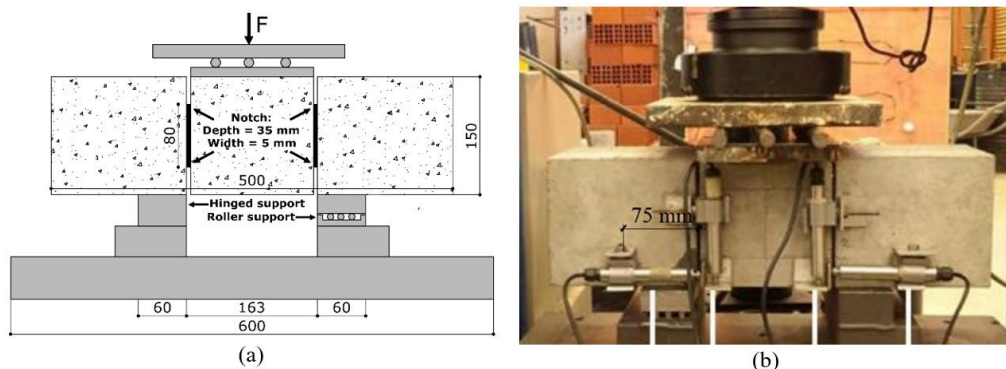


Figure 1. (a) Double-notched push-through test setup (dimensions in mm) and (b) instrumentation.

2.2 Push-off tests

Six Z-type push-off specimens with dimensions of 160 × 250 × 612 mm were cast. Three specimens were prepared using a plain concrete (F-00-2) and another three using a concrete mixture with 1.5% steel fibers (F-15-2). Coarse aggregate with a maximum dimension of 12.5 mm was used. Steel fibers with a hooked end and a circular cross-section were used. According to the manufacturer, the fiber length is 35 mm, the diameter is 0.55, and the aspect ratio is 64. The minimum tensile strength of fibers was 1150 MPa. The mechanical properties of the concrete used in these tests are also shown in Table 1. In these specimens, the shear plane measured 120 × 120 mm.

Specimens were reinforced with a pair of 6.3 mm diameter stirrups (connectors) oriented normal to the shear plane. These stirrups were used to provide normal stress to the shear plane during the test. Adhesion between stirrups and concrete was eliminated near the shear plane in order to reduce its influence on crack dilatancy and shear strength resulting from the dowel action of the bar. This was achieved by wrapping the bar with scotch tape and grease at a distance of 120 mm from the shear plane. A previous study [7] suggested that this procedure is adequate to eliminate the dowel action of the reinforcement, which would only contribute to the normal compression of the shear plane. Strain gages were placed on the stirrups, near the shear plane, to measure the strain of bars during the test.

Push-off tests were conducted in two steps. In the first step, the shear plane of specimens was pre-cracked by applying a splitting load. On both sides of the specimens, there was a 20 mm deep notch where two knives were positioned to induce the pre-cracking of the shear plane. This procedure is similar to one previously described [21]. Loading was applied by displacement control at a rate of 0.010 mm/min until an average crack width of 0.10 mm was produced in the shear plane. Then, the rate was decreased to 0.005 mm/min and kept constant until the average crack width reached about 0.30 mm. Shear crack width was measured using three linear transducers and a clip gage, as shown in Figure 2. Measurements were taken in loading and unloading stages. The strain in stirrups was also measured during this step. It was verified that the stirrup stress did not reach the yield strength of steel on any of the specimens; i.e., all stirrups remained within the linear elastic regime in this first step of the test.

In the second step, the specimen was placed under an electromechanical machine. Load was applied to the top side of the specimen. A roller bearing was attached between plates positioned on the lower side of the specimen to avoid any external horizontal restraint of crack dilatancy during the test. Loading was applied by displacement control at the following rates: 0.004 mm/min for 3 min, 0.02 mm/min until the maximum load was achieved, and 0.05 mm/min until the end of the test.

Four horizontal and two vertical linear transducers were used to measure crack width (w) and the average slip of the shear plane. All instrumentation had an accuracy of 0.01 mm. The instrumentation layout is shown in Figure 3.

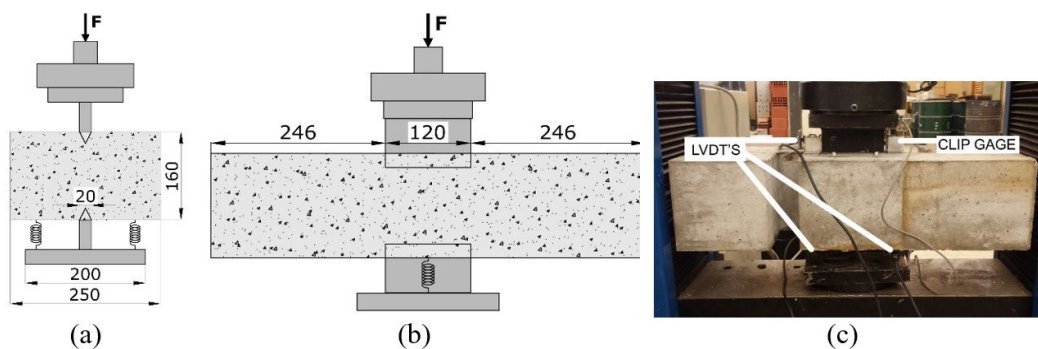


Figure 2. Test setup in the pre-cracking stage: (a) frontal view of specimen (dimensions in mm), (b) lateral view of specimen (dimensions in mm), and (c) splitting test.

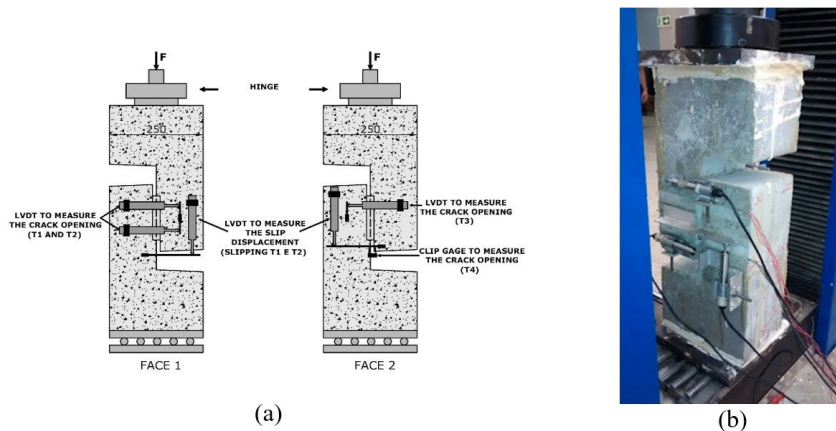


Figure 3. Push-off test instrumentation: (a) front and opposite faces and (b) test setup in the push-off stage.

3 FINITE ELEMENT ANALYSIS OF DIRECT SHEAR TEST RESULTS

In this study, finite element analysis was performed using the commercial software DIANA FEA 10.1 [22], which includes several constitutive models for concrete and masonry.

3.1 Double-notched push-through specimen

A 3D finite element model with a smeared crack approach was used to model specimen with F-00-2 mixture, as shown in Table 1. The objective of this analysis was to determine values for the shear retention factor (β) of concrete without steel fibers.

3.1.1 Mesh, material properties, and loading

The geometry and constraints of the finite element model match those of test supports, as shown in Figure 4. The geometry in black represents specimen supports and the load plate (upper side) on which displacement was imposed. The geometry in red illustrates the notch region. Points *a* and *b*, in green, were used to determine the relative slip of the shear plane.

Because of finite element size limitations imposed by the notch width, which limits the finite element size to 5 mm in the notch region, a regular mesh with 5 mm elements was used. The isoparametric elements with linear interpolation (HX24L element type) were used to model concrete and steel plates, resulting in a total of 98,130 elements in the computational model.

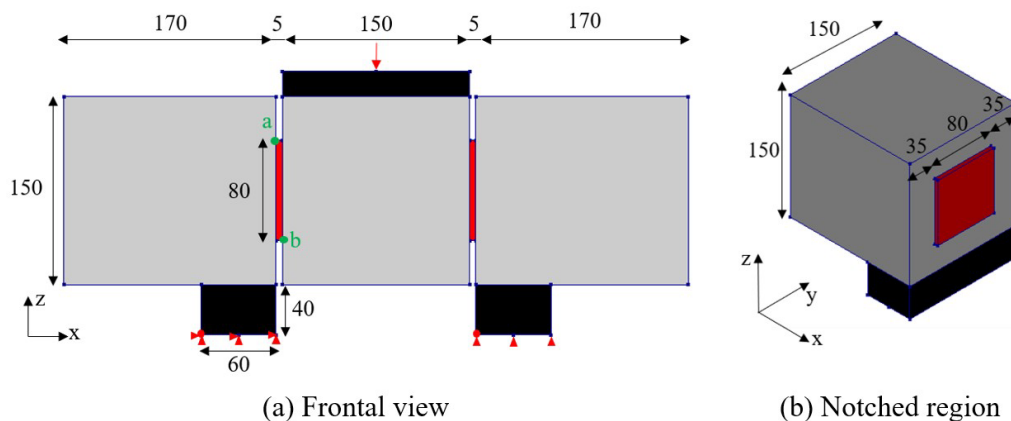


Figure 4. Geometry of the double-notched push-through specimen with uncracked planes (dimensions in mm).

Concrete was described by a total strain model with fixed crack. The equation proposed in Section 5.1.8.1 of Model Code 2010 [23] was used to define the uniaxial compressive behavior of concrete. The uniaxial tensile behavior of concrete without steel fiber was modeled as a linear softening model based on mode I fracture energy. Table 1 shows the values of compression strength, uniaxial tensile strength, modulus of elasticity, and mode I fracture energy determined experimentally. The steel plates used as supports and for applying loads were modeled assuming a linear elastic behavior with a modulus of elasticity of 210 GPa and a Poisson's ratio of 0.3.

Analyses were run in displacement control mode to obtain a post-peak response. Displacement was imposed in 33 steps of 0.03 mm in the *z*-direction, resulting in a total displacement of 0.99 mm on the upper face of the specimen. The maximum slip values observed in the tests were much lower than this value. The quasi-Newton iteration method, based on the Broyden-Fletcher-Goldfarb-Shanno (BFGS) algorithm, was used to reduce processing time, with a maximum of 40 iterations per load step. A convergence criterion based on an energy criterion with a tolerance of 0.1% was used as it is often easier to satisfy than the force criterion.

3.1.2 Result analysis

A parametric study was conducted for different values of the β factor, which was considered constant. Figure 5a shows the relationship between shear stress and shear slip measured using the finite element model. As expected, this

figure indicates an increase in shear resistance as the β values increase. Figure 5b presents the outcomes obtained using the variable shear retention factor suggested by Al Mahaidi [15], Figueiras [16], Rots and Blaauwendraad [17], and Červenka *et al.* [18]. It was noted that different equations for the β factor may influence shear behavior, including the maximum shear stress of the shear plane.

Because of the roller support used in the test, there was no impediment to crack dilatancy in the shear plane after matrix cracking. Therefore, the reduction in the shear stiffness of the shear plane was estimated by measuring the crack width in the shear plane adjacent to the roller support of the specimen with mixture F-00-1, as shown in Figure 6. Table 2 and Figure 7a present a proposed trilinear model for the β factor. Before concrete cracking, full shear retention should be employed ($\beta = 1$). After concrete cracking, the β factor was adjusted according to the decrease in the slope of the relationship between shear stress and crack width observed in the test data (Figure 6). A minimum β factor of 0.01 was set, and an ultimate normal strain of 0.0045 was admitted, in accordance with values used by several authors, such as Figueiras [16] and Rots and Blaauwendraad [17].

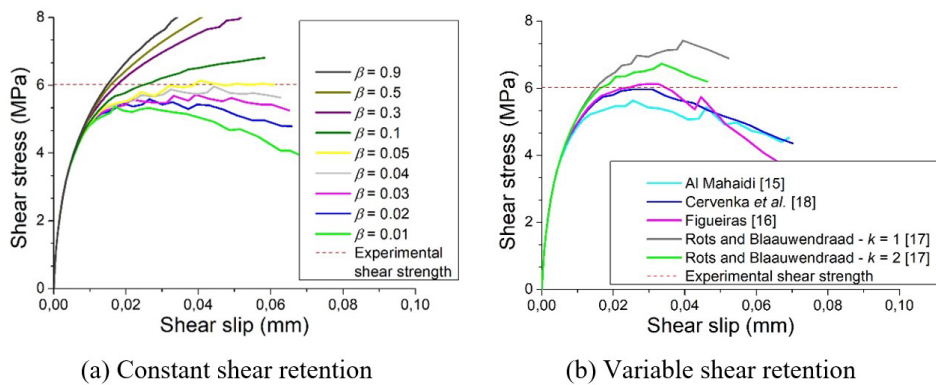


Figure 5. Influence of (a) constant shear retention factor and (b) variable shear retention factor on double-notched push-through test results (F-00-2).

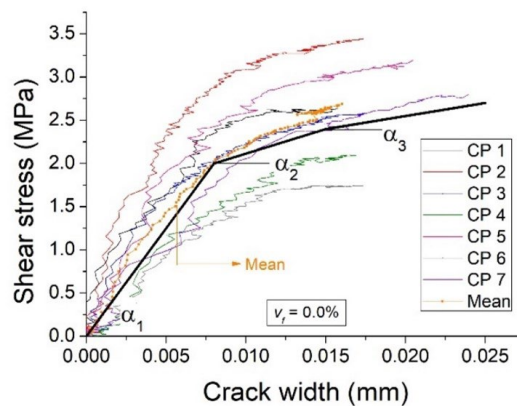


Figure 6. Relationship of shear stress and crack width in double-notched push-through tests (F-00-1).

Table 2. Empirical values of variable shear retention factor (β) estimated from double-notched push-through test results (F-00-1).

Stage	Shear stress (τ) (MPa)	Crack width (w) (mm)	α (MPa/mm)	β	Normal strain (ϵ_{nn}) $\times 10^{-3}$
1	2.0	0.008	250	1	0.107
2	2.4	0.015	57	0.228	0.200
3	-	-	-	0.01	4.500

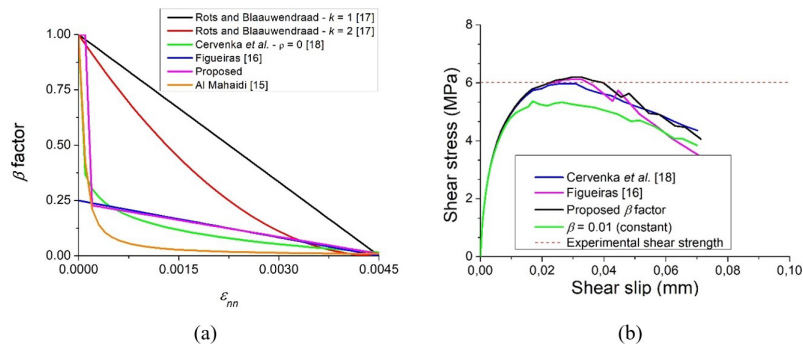


Figure 7. (a) Proposed equations for the variable shear retention factor (β) and (b) shear stress–slip curves obtained using the finite element model and several variable shear retention equations.

Despite the roller support not applying normal stress on the shear plane, the acting and reaction forces were not aligned, resulting in bending in the shear plane. Consequently, the crack width measured on the bottom face of the specimen was divided by the distance between the neutral axis and the position of the horizontal linear variable displacement transducer (LVDT) during the elastic phase to obtain the strain. In the test setup, this distance is approximately half the height of the specimen, or 75 mm. Table 2 shows the normal strain and corresponding β factor, which were determined based on the reduction of stiffness (α) in the relationship between shear stress and crack width (or normal strain) presented in Figure 6. In the first stage, β factor was assumed to be 1 because the value of the normal strain at the end of this stage ($\tau = 2$ MPa) is close to the theoretical elastic distortion strain for concrete, i.e., $\gamma = \tau / G = 0.126 \times 10^{-3}$. For this analysis, G was adopted as $E / [2(1 + \nu)] = 15817$ MPa, where the coefficient of Poisson (ν) was assumed to be 0.2. Therefore, in the first stage, the slope would be close to the elastic shear modulus of the concrete used in the tests.

Figure 7a shows the final proposed curve for the β factor. In the figure, the curve is compared with other shear retention curves available in the literature. The empirical β factor determined experimentally exhibits similar behavior to the equations suggested by Figueiras [16] and Červenka et al. [18], which demonstrate the effectiveness of the test setup used in this analysis for estimate the values of the β factor. This was possible because, without normal stress confining the shear plane and assuming a plane strain state, the maximum shear strain can be assumed to be approximately equal to the maximum normal strain measured by the LVDT. Figure 7b shows the relationship between shear stress and shear slip estimated by the finite element model using several variable shear retention equations, including the β factor suggested in this study. The use of the empirical β factor and the other two equations for variable shear retention factor results in no significant difference in the curves.

Table 3 presents the maximum resistance load of specimens obtained from both the tests and finite element analysis. With the use of the empirical β factor suggested in this study, as well as the equations proposed by Figueiras [16] and Červenka et al. [18], a difference of less than 5% was observed in the maximum load between the finite element analysis and test results, indicating the similarity between these three proposed formulations for variable β factor. It is noteworthy that the difference of less than 5% with constant shear retention was also obtained with a β factor of approximately 0.05.

Table 3. Maximum resistance load of the double-notched push-through specimen.

Shear retention factor	Maximum load (kN)	Difference from test result
Experimental result (F-00-2)	79.62 ± 3.2	-
$\beta = 0.01$ (constant)	68.71	-13.70%
$\beta = 0.02$ (constant)	71.15	-10.64%
$\beta = 0.03$ (constant)	73.28	-7.96%
$\beta = 0.04$ (constant)	76.41	-4.03%
$\beta = 0.05$ (constant)	78.62	-1.25%
Al Mahaidi [15] (variable)	70.51	-11.44%
Červenka et al. [18] (variable)	76.79	-3.55%
Rots and Blaauwendraad, $k = 1$ [17] (variable)	95.04	19.37%
Rots and Blaauwendraad, $k = 2$ [17] (variable)	86.17	8.23%
Figueiras [16] (variable)	78.41	-1.52%
Proposed β factor (variable)	79.43	0.24%

3.2 Push-off specimens

In this phase of the study, aggregate interlock resistance was modeled using the discrete crack approach with the interface elements available in DIANA FEA 10.1 software. The same method was used by Blomfors et al. [24] to simulate beams without stirrups and with pre-existing cracks. However, the authors used a three-dimensional model and did not explicitly consider aggregate interlock resistance. In this study, two-dimensional plane stress was used because of the limitation of the software version, which only contained analytical equations for crack dilatancy in two-dimensional interface elements.

3.2.1 Mesh, material properties, and loading

The geometry of the push-off specimen is shown in Figure 8, with translational constraints in the x -direction on the right face of the specimen and in the y -direction at the base. In this configuration, the left L-shaped block is free to move along the x -direction, as it was during the test.

Stirrups are represented by L2TRU truss elements inserted across the shear plane. In the shear plane, given the elimination of adhesion, truss elements had no connection with concrete elements of the mesh. The physical thickness of the specimen is 160 mm; however, the finite element model is only 120 mm thick, which is the thickness of the shear plane.

The mesh of concrete and steel plates is composed of plane stress elements with quadratic interpolation (CQ16M type). The finite element size was set at 25 mm (Figure 8). The constructive reinforcement of the model was represented by embedded reinforcement. Within the shear plane, interface elements that incorporate some analytical equations of aggregate interlock were used (CL12I type).

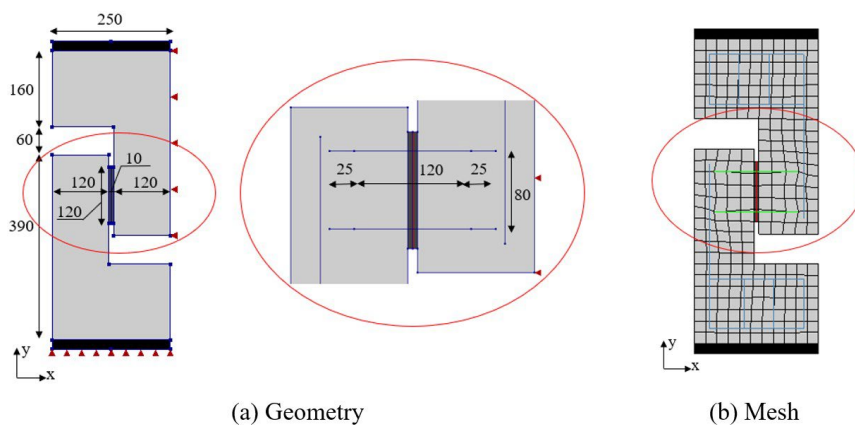


Figure 8. Push-off specimen with pre-cracked shear plane (dimensions in mm).

The mechanical properties of plain (F-00-2 mixture) and fiber-reinforced concrete (F-15-2 mixture) are presented in Table 1. The constitutive law used to model the push-off plain concrete specimen is the same as that described by the finite element model of the double-notched push-through specimen with the variable shear retention factor proposed in this study.

Embedded reinforcements were assumed to have linear elastic behavior, with a modulus of elasticity of 210 GPa, representing the steel used as constructive reinforcement. The truss elements that cross the shear plane were assumed to have non-linear behavior, which was determined from a characterization test of the steel. The modulus of elasticity of the reinforcement was set at 202 GPa, also obtained from the steel characterization test.

Normal and tangent stiffnesses of interface elements were defined by inverse analysis: the values for the finite element model that best matched the initial stiffness were selected. Normal stiffness was found to be 1×10^8 N/mm; and tangential stiffness, 1×10^6 N/mm.

Aggregate interlock was considered in the interface element of the finite element model. Thus, crack dilatancy, which is more advanced than standard discrete cracking for sliding along rough macro-cracks, was used in interface elements. The parameters of the crack dilatancy model were maximum aggregate size (12.5 mm), compressive strength, and mode I fracture energy (values shown in Table 1). Given that the shear plane was pre-cracked before the direct shear test, the tensile strength of the interface was assumed to be zero. The software contains various models for aggregate interlock in two-dimensional interface elements. Variation of the crack dilatancy model did not influence the

results of computational modeling; therefore, the two-phase model proposed by Walraven and Reinhardt [7] was applied to the current finite element model.

A bilinear tension softening diagram was constructed for finite element modeling of the push-off specimen with steel fiber-reinforced concrete. The stress–strain diagram of steel fiber-reinforced concrete was obtained through inverse analysis of toughness test results of F-15-2 mixture, which was performed according to ASTM C1609 [25]. In the referred test, an unnotched prismatic specimen ($150 \times 150 \times 500 \text{ mm}^3$) is bent by four-point loading. Inverse analysis consists in generating a stress–strain diagram via computational modeling of toughness test data, providing a load–displacement curve similar to the curve obtained from the test.

It is worth noting that the smeared crack approach assumes that the deformations of a single crack can be distributed over a characteristic length (l_c). In the case of plain reinforced concrete modeling, this characteristic length is approximately equal to the size of one finite element. For steel fiber-reinforced concrete, the same assumption can be made, but some considerations may be required when modeling a combination of fiber-reinforced concrete and conventional reinforcement. When cracks are distributed throughout the structure, rather than localized to a specific crack, the characteristic length may need to be adjusted. If the crack pattern is unrealistic and too many elements are cracked, the ductility and load resistance can be overestimated if the characteristic length is assumed to be the size of one finite element. In this scenario, the characteristic length should be selected as the size of multiple elements, but not exceeding the average expected crack spacing [26]. For this reason, the mesh size used in the inverse analysis of the prismatic specimen was chosen to be the same as that used in the finite element modeling of the push-off specimen, which was 25 mm. Therefore, the characteristic length was not determined in this analysis and the stress–strain diagram obtained is specific to this mesh size. It should be adjusted using an appropriate characteristic length for other mesh sizes.

Figure 9a and Table 4 show the bilinear tension softening diagram of steel fiber-reinforced concrete obtained by inverse analysis. Figure 9b compares the load–displacement curve obtained from the ASTM C1609 test [25] to that of the finite element model. The area under the curve of the inverse analysis differed in less than 5% from the area under the curve of the test.

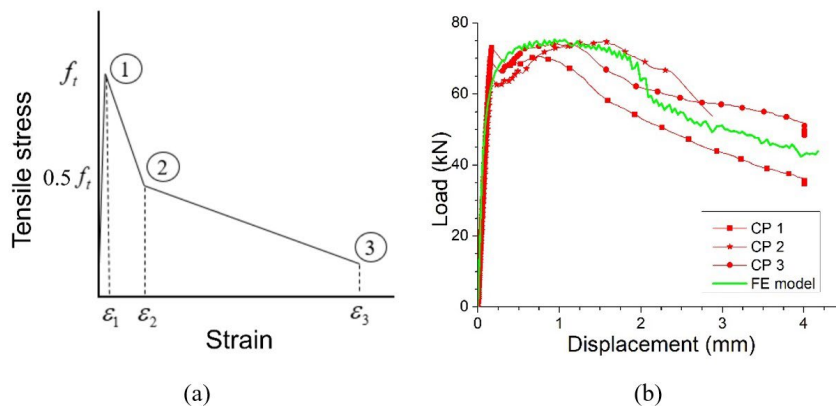


Figure 9. (a) Bilinear tension softening diagram for steel fiber-reinforced concrete and (b) load–displacement curve obtained according to ASTM C1609 for F-15-2 mixture.

Table 4. Points of the bilinear tension softening diagram for steel fiber-reinforced (F-15-2 mixture).

Point	Tensile stress (MPa)	Total strain ($\times 10^{-3}$)
1	3.93	0.09
2	1.80	50
3	0.7	1000

Analyses were also run under displacement control to obtain the post-peak response. Displacement was imposed with 400 steps of 0.005 mm in the y-direction, resulting in a total displacement of 2 mm on the upper face of the push-off specimen. The maximum slip values observed in the tests were close to this value. The quasi-Newton iteration method based on the BFGS algorithm was also used, but the maximum iterations per load step were increased to 1000 due to the difficulty in satisfying the convergence criterion with the interface elements. In this analysis, a convergence criterion based on an energy criterion with a tolerance of 0.1% was also used.

3.2.2 Result analysis

Figure 10 shows the relationships between shear stress, normal stress, crack width, and shear plane slip for the push-off specimen without steel fibers (F-00-2 mixture). For a crack width of zero, the stiffness predicted by the finite element model was equal to experimental values. For increasing crack widths, the model curve ranged within the limits of test curves. The maximum shear stress predicted by the finite element model (6.89 MPa) showed reasonable agreement with the average stress obtained from the test (6.99 MPa), differing by only 1.4%.

The finite element model had a similar behavior to the experimental specimen. It is noted that, in the initial stage, normal stress was low and there was no crack width on the shear plane. Then, the normal stress across the crack increased with crack width and shear slip at the interface. Normal reinforcement did not yield when the maximum shear stress was reached, different from the observed in the test specimen. Nevertheless, the finite element model successfully simulated the relationship between experimental shear stress and normal stress up to the maximum shear stress.

As observed in the test, steel fibers increased shear strength according to the finite element model (Figure 11). The maximum shear stress estimated by the finite element model was 9.46 MPa, being 8.5% lower than the average value obtained in the test (10.34 MPa). The finite element model adequately predicted crack width evolution up to the maximum shear stress but differed from experimental specimens in the post-peak stage, given that the DIANA FEA analysis does not consider steel fibers in aggregate interlock models. As explained by Araújo et al. [3], steel fibers crossing the shear plane begin to contribute to shear strength only after the maximum aggregate interlock capacity is reached, and their contribution depends on maximum aggregate size.

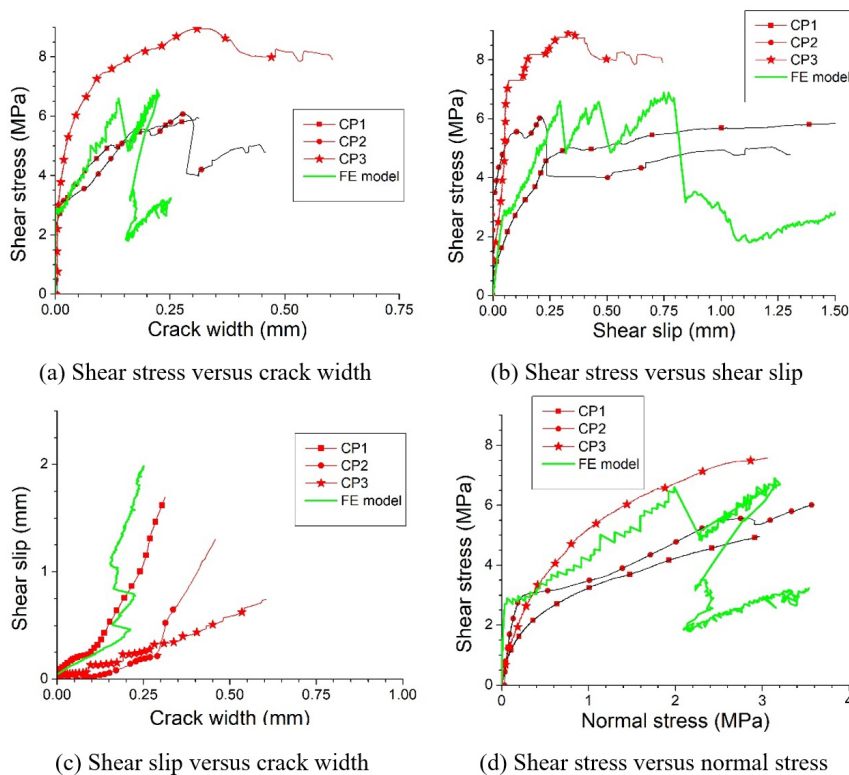


Figure 10. Relationship curves for the push-off specimen without steel fibers (F-00-2).

A good correlation between experimental and model results for the normal stress versus shear stress curve was observed up to maximum shear stress, even though the finite element model showed a smaller crack width in the shear plane. After this, the finite element model showed a decrease in shear stress, which was not observed in the test specimen because of the normal reinforcement. It is concluded that the finite element model was able to accurately represent the push-off specimen with steel fiber-reinforced concrete only up to the maximum shear stress because the finite element model did not consider the presence of steel fibers crossing the cracked plane. Previous studies explicitly

simulated steel fibers in the cracked plane in mode I fracture but did not consider the interaction between fibers and aggregate interlock in the cracked plane [27]. Other studies have analyzed the interaction between steel fibers and aggregate interlock and proposed analytical solutions, but did not present computational modeling [28], [29]. Some other studies have proposed constitutive models for fiber-reinforced concrete by coupling the fiber and the aggregate interlock, but they have not correlated their results with the shear retention factor [30], [31].

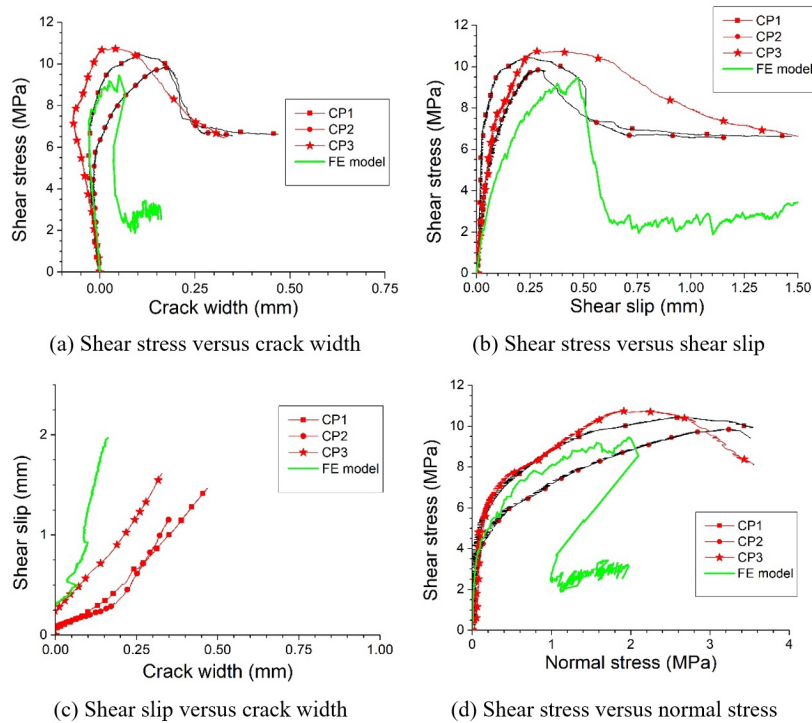


Figure 11. Relationship curves for the push-off specimen with steel fibers (F-15-2).

Despite the limitations of the finite element model in simulating aggregate interlock with steel fibers, it was able to predict the influence of steel fibers on the shear strength (Figure 12). Therefore, an interface element with crack dilatancy models associated with the tensile behavior of steel fiber-reinforced concrete can be used to simulate a push-off specimen of fibrous concrete with a pre-cracked shear plane only up to the maximum shear stress. More studies should be conducted on the representation of the crack shear modulus of steel fiber-reinforced concrete through a shear retention factor, primarily to characterize the mode II fracture parameter of the steel fiber-reinforced concrete.

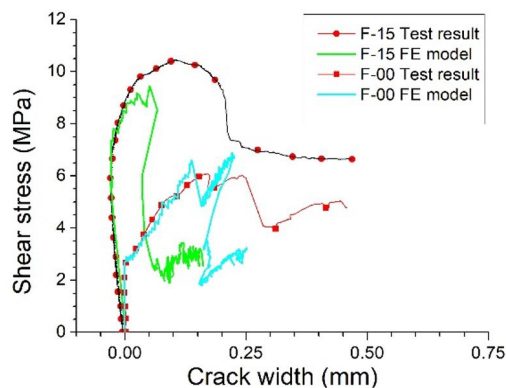


Figure 12. Shear stress versus crack width for push-off specimens with and without steel fibers.

4 FINITE ELEMENT MODEL OF REINFORCED CONCRETE BEAMS WITHOUT STIRRUPS

In the current study, two approaches were used to model the shear strength of reinforced concrete beams with a shear span-to-depth ratio (a/d) less than 3 and no transverse reinforcement, under plane stress. Two beams tested by Araújo et al. [32] and one beam tested by Garcia [33] were used. Of the beams tested by Araújo et al. [32], the V-0-0 and V-1-0 beams were selected, which had a shear span-to-depth ratio (a/d) of 2.17. The first beam was composed of plain concrete, and the second beam contained 1% steel fibers, similar to the fibers used in the experimental procedure presented in item 2. Both beams had a maximum aggregate size of 12.5 mm (Figure 13a). Of the beams tested by Garcia [33], the beam 1R was selected, which had a shear span-to-depth ratio (a/d) of 2.66, no steel fibers, and maximum aggregate size of 19 mm (Figure 13b).

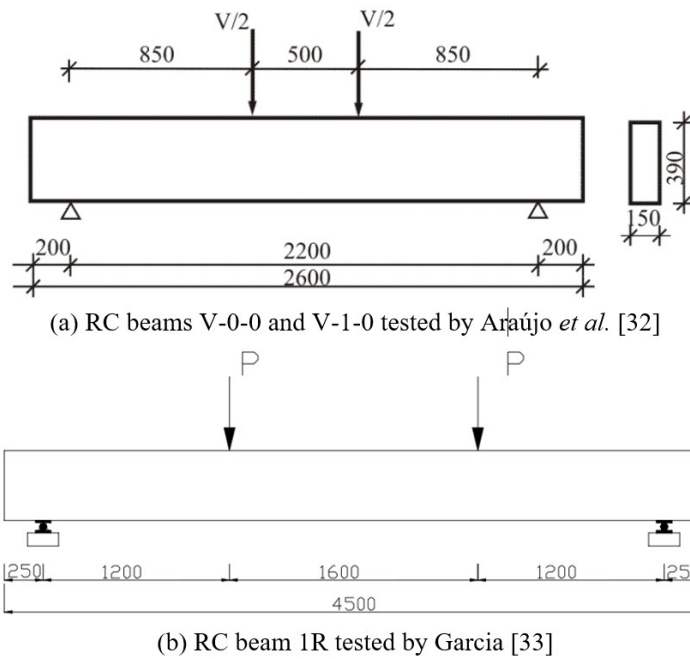


Figure 13. Geometry of reinforced concrete (RC) beams used for modeling (dimensions in mm).

These beams cover two types of potential shear failure. Beams with shear span that are short, with an aspect ratio (a/d) ranging from 1 to 2.5, develop inclined cracks near the supports and can support loads through arch action. The ultimate failure of these beams occurs due to a splitting failure or crushing of the compression zone over the top of the crack, which is referred to as shear compression-failure. In shear spans that are slender, with an aspect ratio ranging from about 2.5 to about 6, the beam fails with inclined cracks due to the combined effect of shear force and bending moment. This failure type mobilizes several mechanisms in the reinforced concrete beam, such as cantilever action, residual tensile strength action, dowel action, and aggregate interlock [34, 35].

4.1 Finite element mesh

In the finite element model with a discrete crack approach, the shear crack in reinforced concrete beams was described by interface elements, and aggregate interlock was represented by the crack dilatancy model. This modeling approach was used only for beams with plain concrete, as finite element modeling results of the push-off specimen demonstrated that aggregate interlock models did not accurately represent the post-peak behavior of specimens with steel fiber-reinforced concrete. For all reinforced concrete beams, only the mid-span was modeled, given the symmetry of the beam and the applied loading.

A shear crack with an angle of 42° was observed in V-0-0 beam, which started from the point of applied load up to the longitudinal reinforcement on the lower face of the beam. The finite element mesh shown in Figure 14a was generated, where red lines represent the interface elements used to simulate the shear crack of the beam. In the smeared crack approach, the beam had the same finite element mesh as in the discrete crack approach but without interface elements to simulate the shear crack (see Figure 14b). The size of finite elements was 10 mm in both approaches for the V-0-0 beam. The mesh for the V-1-0 beam was identical, with the exception that only the smeared crack approach was used to model this beam.

During testing of beam 1R, a shear crack with an angle of 45° was observed, and a finite element mesh (shown in Figure 15a) was developed. Interface elements were also used to model the shear crack. Figure 15b shows the mesh used in the smeared crack approach. Each finite element mesh had a dimension of 10 mm. All beams were modelled using a finite element with quadratic interpolation. Beam reinforcements were represented by embedded reinforcement elements.

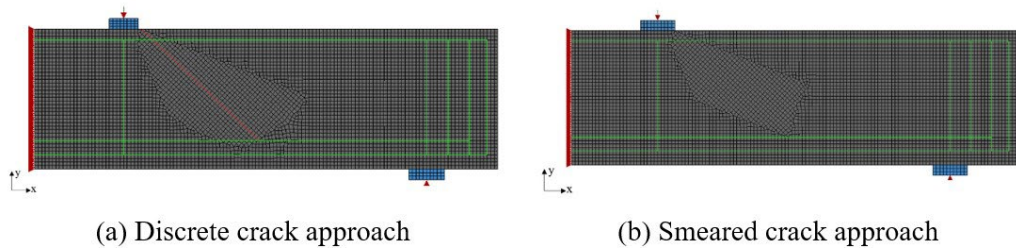


Figure 14. Finite element mesh of reinforced concrete beam V-0-0.

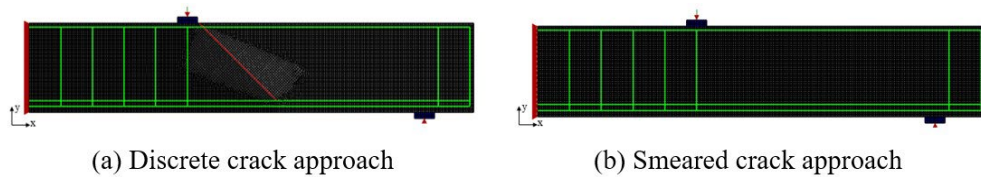


Figure 15. Finite element mesh of reinforced concrete beam 1R.

4.2 Material properties and constitutive laws

The mechanical properties of plain concrete and steel fiber-reinforced concrete beams are described in Table 5, and the mechanical properties of beam reinforcements are given in Table 6.

The compressive behavior of concrete was modeled using a parabolic curve based on fracture energy, and the tensile behavior of plain concrete was modeled using a linear softening diagram based on mode I fracture energy. For plain concrete, the crack bandwidth was automatically calculated as the square root of the finite element area, according to the method proposed by Rots [36]. The compressive fracture energy was defined as 100 times the mode I fracture energy.

Table 5. Mechanical properties of concrete.

Beam	Fiber content (%)	Coarse aggregate (mm)	f_c (MPa)	f_{ct} (MPa)	E_c (GPa)	G_f^I (N/mm)	G_c (N/mm)	ν
V-0-0	0.00	12.50	46.30	3.70	27.73	0.146	14.6	0.3
V-1-0	1.00	12.50	56.87	3.28	31.78	Table 6	341.1	0.3
1R	0.00	19.00	70.20	3.24	28.82	0.156	15.59	0.3

f_c : compressive strength of concrete; f_{ct} : axial tensile strength of concrete; E_c : modulus of elasticity of concrete; G_f^I : fracture energy of concrete; G_c : compressive fracture energy of concrete; ν : Poisson's ratio of concrete.

Table 6. Mechanical properties of beam reinforcements.

Beam	1R	V-0-0 and V-1-0
Bar diameter (mm)	6.3	20.0
Modulus of elasticity (GPa)	173.33	210.00
Yield strength (MPa)	390	500

The tensile behavior of the steel fiber-reinforced concrete in the V-1-0 beam was represented by a bilinear tension softening diagram, as shown in Figure 9a. The stress and strain values for this diagram were obtained by Araújo et al. [5] using an inverse analysis on prismatic specimens under four-point loading, as presented in Table 7. The compressive fracture energy was defined as 100 times the area under the tensile stress-strain curve multiplied by the crack bandwidth, which was adopted as the size of the finite element (10 mm).

Table 7. Bilinear tension softening of the steel fiber-reinforced concrete of beam V-1-0.

Point	Tensile stress (MPa)	Strain (%)
1	3.28	0.103
2	1.64	12.00
3	0.00	50.00

The same stiffnesses that were determined by finite element analysis of the push-off test were applied for the discrete crack approach using interface elements. However, for beams, the tensile strength of the interface element was assumed to be equal to the tensile strength of concrete, given that the shear plane of beams was not previously cracked. Different crack dilatancy models in interface elements were used for computational modeling of beams.

4.3 Result analysis

Table 8 shows the maximum load of beams obtained using the smeared crack approach and different values for the shear retention factor (β). The use of the empirical β factor proposed in this study (Table 2) allowed good representation of the maximum load of the two test beams without fibers. The equation proposed by Al Mahaidi [15] has a similar variation of the empirical β factor and also displays good precision in evaluating the maximum load of beams without fibers. The equations proposed by Figueiras [16] and Červenka et al. [18] allowed good representation of the maximum load of the beams V-0-0 and 1R, respectively. For V-1-0 beam with steel fiber-reinforced concrete, the equations proposed by Červenka et al. [18] and Figueiras [16] and the empirical β factor proposed in this study (Table 2) predicted the maximum load of steel fiber-reinforced concrete beams with an error of less than 10%.

Table 8. Maximum load of beams estimated by the finite element model using the smeared crack approach.

Shear retention factor	V-0-0		V-1-0		1R	
	Maximum load (kN)	Difference from test	Maximum load (kN)	Difference from test	Maximum load (kN)	Difference from test
Experimental result	172.50	-	260.00	-	133.00	-
$\beta = 0.01$	145.66	-15.56%	276.77	6.45%	153.67	15.54%
$\beta = 0.05$	153.95	-10.75%	263.97	1.53%	128.75	-3.20%
$\beta = 0.10$	153.77	-10.86%	248.54	-4.41%	127.46	-4.17%
$\beta = 0.30$	184.76	7.11%	287.71	10.66%	132.88	-0.09%
Al Mahaidi [15]	169.05	-2.00%	170.10	-34.58%	135.62	1.97%
Červenka et al. [18]	198.95	15.33%	279.78	7.61%	128.07	-3.71%
Rots and Blaauwendraad, $k = 1$ [17]	204.11	18.32%	231.34	11.02%	128.56	-3.34%
Figueiras [16]	177.13	2.68%	248.54	-4.41%	105.10	-20.98%
Proposed β factor	174.47	1.14%	282.44	8.63%	138.74	4.32%

When a constant β factor is used, the resistance of the finite element model usually increases with increasing β . However, there is no unique value that can be used to accurately estimate the strength of the three beams, and the best prediction for each beam was obtained with different β values.

Table 9 describes the results obtained using the discrete crack approach, represented by interface elements, for beams without steel fiber-reinforced concrete. The models for crack dilatancy proposed by Walraven and Reinhardt [7] and Li et al. [9] were the ones that best predicted the maximum load for V-0-0 beam. For beam 1R, all models predicted the maximum load of the beam with an error of less than 10%.

Figure 16 compares the load–displacement curves of the V-0-0 beam obtained from the experimental test and the finite element model using the two approaches. For low constant β factor values, the stiffness of the cracked beam estimated by the finite element model was found to be similar to the initial experimental stiffness, but the maximum load of the beam was lower. By contrast, the finite element model with the variable β factor estimated the maximum load of the beam with more precision. However, it also exhibited less displacement than was observed during the test after the formation of the flexural cracks. On the other hand, the finite element model with a discrete crack approach accurately represented the cracking shear load of the beam. i.e., 96.2 kN in the model compared to 87.5 kN in the test. Furthermore, beam stiffness was accurately represented after formation of the shear crack. It is important to note that

vertical beam displacement was not measured up to the maximum load; thus, the analysis refers to the loading where the vertical displacement was measured in the test.

Table 9. Maximum load of beams estimated by the finite element model using the discrete crack approach.

Crack dilatancy model	V-0-0		1R	
	Maximum load (kN)	Difference from test	Maximum load (kN)	Difference from test
Experimental result	172.50	-	133.00	-
Li et al. [9]	164.05	-4.89%	141.73	6.62%
Walraven and Reinhardt [7]	172.09	-0.24%	140.73	5.71%
Walraven [6]	134.18	-22.21%	137.35	3.27%
Gambarova and Karakoç [8]	155.21	-10.03%	143.62	7.98%

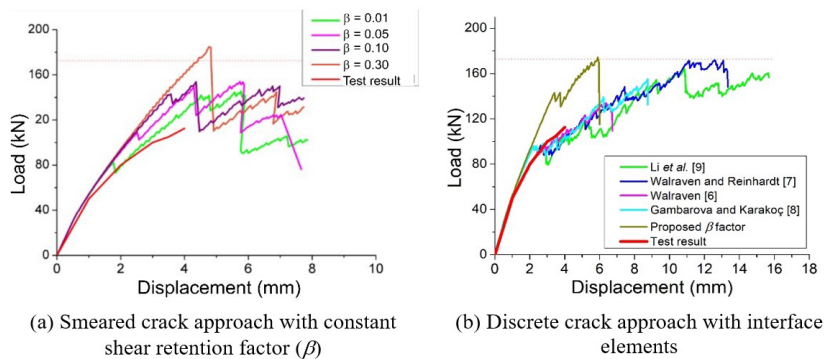


Figure 16. Load–displacement curve of the mid-span of the reinforced concrete beam V-0-0 ($a/d = 2.17$).

The good results of the discrete crack approach with interface elements for representation of the shear crack of the V-0-0 beam can be explained by the crack pattern. Both modeling approaches had a crack pattern similar to that observed at the end of the test (Figure 17); however, the finite element model with the discrete crack approach showed a wider crack width and more sliding along the crack, as simulated by interface elements, than the smeared crack approach. A secondary shear crack was observed, with branches near the point of load application. Hence, the discrete crack approach was capable of providing a more precise estimation of the stiffness of short shear-span beams when failure occurred due to shear-compression with a single shear crack and a low quantity of flexural cracks.

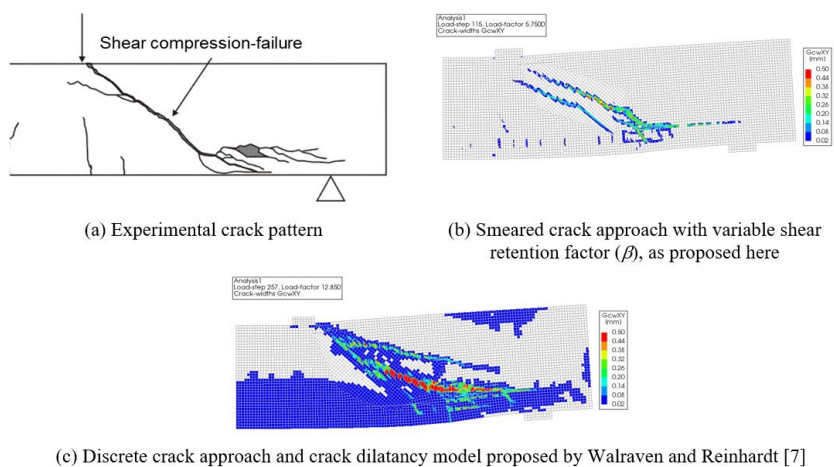


Figure 17. Crack pattern of the reinforced concrete beam V-0-0 ($a/d = 2.17$).

Figure 18 shows the load–displacement curves of beam 1R, which were estimated from the experimental test and the finite element model using two modeling approaches. Overall, minimal variations in maximum load were observed when the smeared crack approach was utilized, regardless of whether a constant β factor ($0.05 < \beta < 0.3$) or a variable β factor. Also, the use of the discrete crack approach with interface elements provided similar maximum load values, regardless of the crack dilatancy model used.

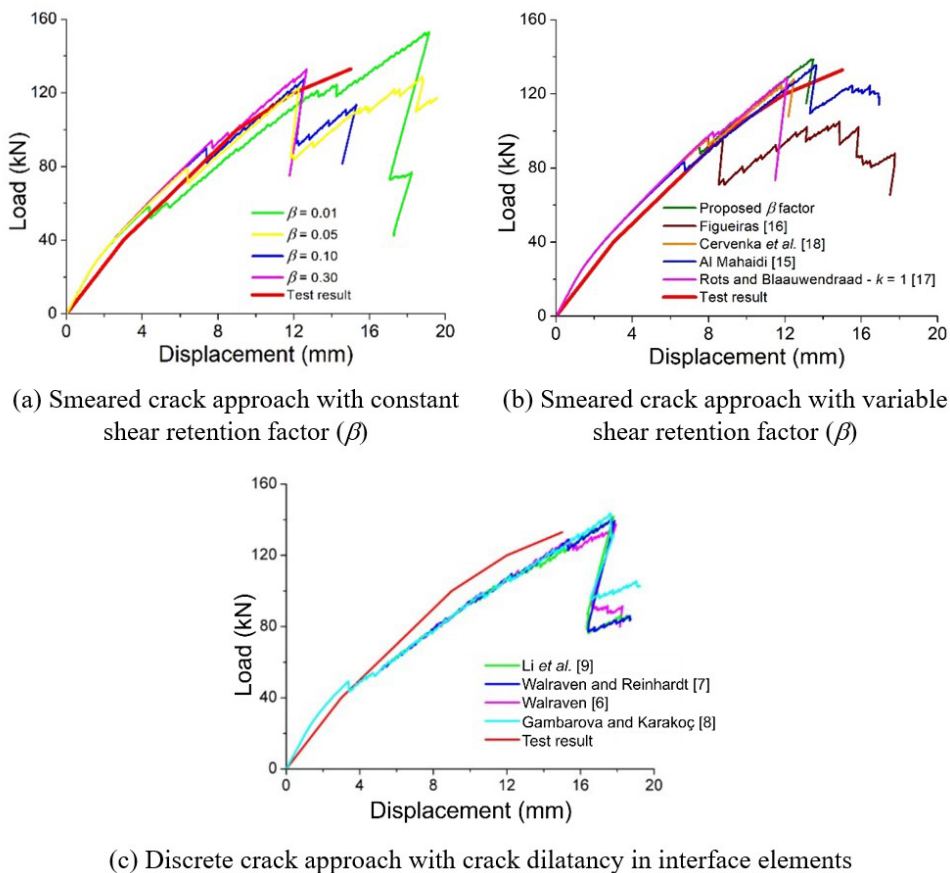


Figure 18. Load–displacement curves of the mid-span of the reinforced concrete beam 1R ($a/d = 2.66$).

The cracking behavior of beam 1R was well represented by both smeared and discrete crack approaches. Such a finding is due to the failure mode of the beam, which has a shear span-to-depth ratio (a/d) of 2.66. Because the concentrated load was further from the support, the beam developed several flexural cracks before the appearance of the main shear crack, which defined the maximum load of the beam (Figure 19). This ensured that beam displacement was not predominantly influenced by sliding along the main shear crack, having a greater contribution from flexural cracks. Thus, the discrete crack approach simulated a main shear crack with the same pattern as that predicted by the smeared crack approach. In this beam, with slender shear-span, the smeared crack approach was sufficient to represent the stiffness of the beam after concrete cracking.

Figure 20 compares the experimental and predicted load–displacement curves of the fibrous concrete beam V-1-0. The smeared crack approach revealed a small influence of the shear retention factor on the response of the beam. The different β factor values afforded similar maximum loads. This finding demonstrates that the tensile behavior of fibrous concrete is more important than the shear retention factor of steel fiber-reinforced concrete beams, even in the case of shear failure.

The crack pattern of beam V-1-0 is depicted in Figure 21. Given that steel fibers provide greater resistance to flexural cracking, there is greater flexural cracking during the test. Thus, although the beam had a shear span-to-depth ratio (a/d) of 2.17, unlike reinforced concrete beam V-0-0 without fibers, the smeared crack approach adequately represented beam stiffness after concrete cracking.

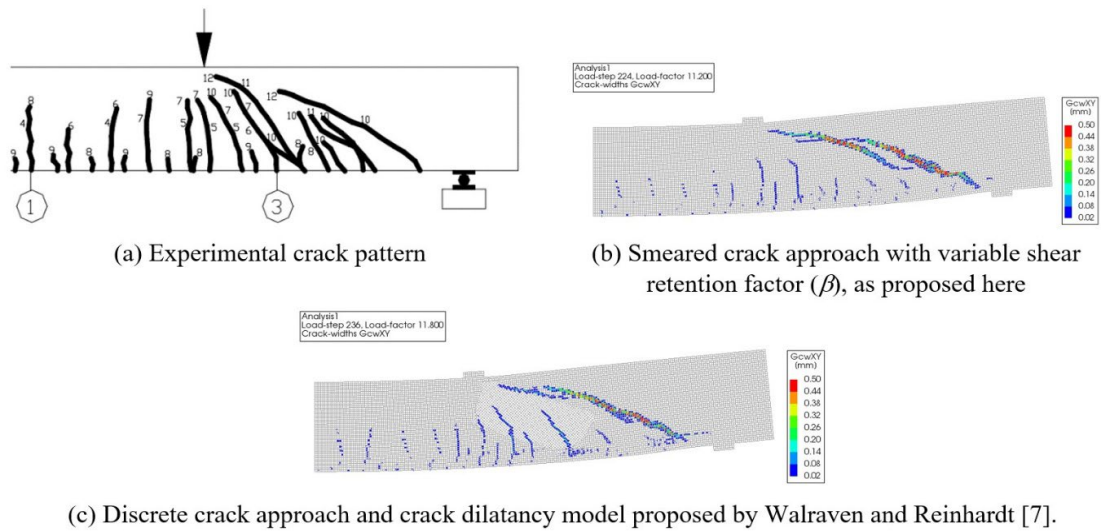


Figure 19. Crack pattern of the reinforced concrete beam 1R ($a/d = 2.66$).

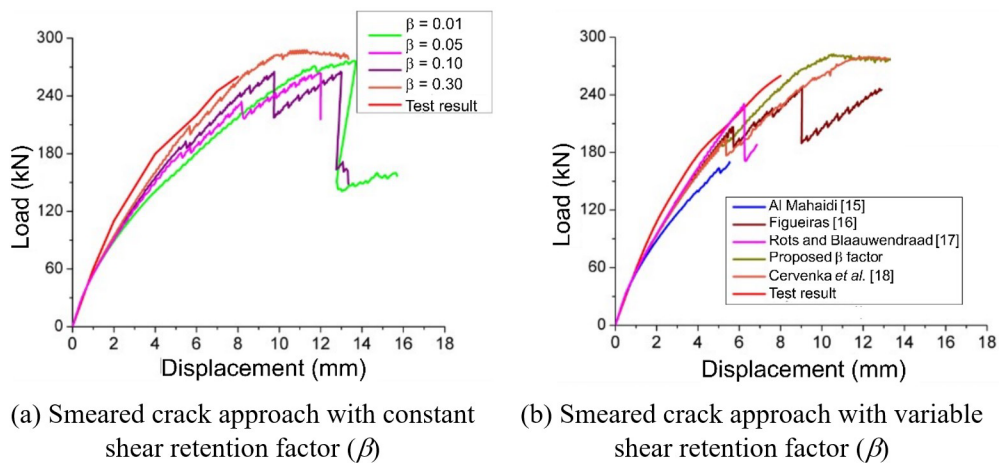


Figure 20. Load–displacement curves of the mid-span of the fibrous concrete beam V-1-0 ($a/d = 2.17$).

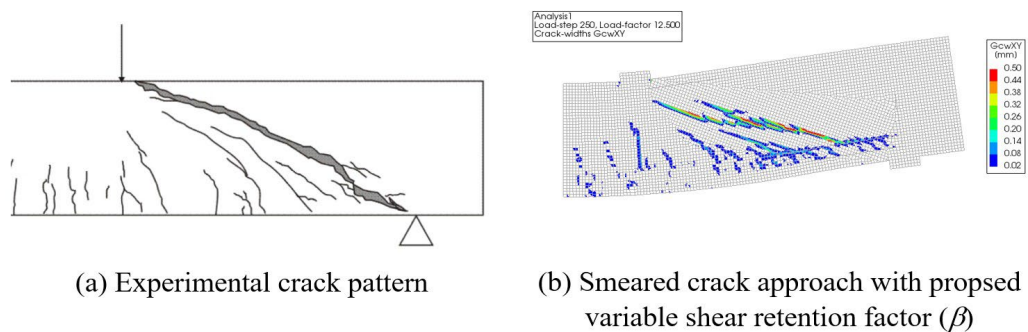


Figure 21. Crack pattern of the fibrous concrete beam V-1-0 ($a/d = 2.17$).

5 CONCLUSIONS

In this study, finite element models were developed to simulate direct shear tests and reinforced concrete beams without transverse reinforcement and with span-to-depth ratios of 2.17 and 2.66. Several shear retention factors (β)

factor) were used to determine their effectiveness. The empirical β factor was deduced from double-notched push-through tests, which predicted well the shear strength of reinforced concrete beams without steel fibers. The behavior of the proposed β factor was similar to the equations proposed by Figueiras [16] and Červenka *et al.* [18], which confirms the effectiveness of the test setup adopted in this study. Furthermore, the variable β factor suggested by Al Mahaidi [15] was also accurate to predict the shear strength of reinforced concrete beams without steel fibers.

On the other hand, when a constant β factor is used, the shear strength of finite element models usually increases as β factor increases. However, there is no unique value that can precisely estimate the shear strength of reinforced concrete beams. This conclusion is consistent with the observations of Hendriks *et al.* [14], who strongly recommended utilizing a variable shear retention factor in fixed crack models. Constant β factor models are not advisable since they tend to overestimate the stiffness of beams and slabs.

A finite element model was developed to simulate push-off specimens with a pre-cracked shear plane using crack dilatancy models implemented in interface elements. Different models for aggregate interlock did not provide significant differences, suggesting that they are equivalent for simulating push-off specimens. Finite element models predicted greater shear slip and lower crack width than that observed in the test, indicating the need for further analysis of the interaction between aggregate interlock, steel fiber, and dowel rebar.

Finite element modeling using the smeared crack approach for beams without transverse reinforcement is a viable alternative for cases where the shear crack fracture is unknown. In this case, the smeared crack approach was precise enough to estimate the resistance, stiffness, and crack pattern of beams without transverse reinforcement and a shear span-to-depth ratio of 2.66. This was due to the densely distributed flexural and shear cracks that governed the overall behavior of the beam.

For beams without transverse reinforcement and with a shear span-to-depth ratio of 2.17, the stiffness of the cracked beam was better represented by the discrete crack approach. These beams exhibited only a few flexural cracks before the appearance of the critical shear crack, indicating that the smeared crack approach is not suitable for accurately representing the overall behavior of these beams. An appropriate solution for beam with shear compression-failure is to use the smeared crack approach as a qualitative predictor of crack localization, followed by a more precise analysis using the predefined crack, which can be represented by the discrete crack approach with interface elements.

For beams with steel fiber-reinforced concrete, the shear retention factor had a slight influence on beam behavior due to the greater ductility in tension of the fibrous concrete. Additionally, different values of the β factor in finite element analysis with the smeared crack approach had little impact on the stiffness and shear strength of the beam. If a constant β factor is used in modeling, a value less than 0.1 is recommended.

It is important to note that these conclusions were obtained from modeling only three beams, and thus, further research should be conducted to confirm these results for beams with different concrete strength and geometry. Nevertheless, these results are a significant contribution to guiding designers in finite element modeling of beams and slabs without transverse reinforcement.

ACKNOWLEDGEMENTS

This study was financed in part by the Brazilian Federal Agency for Support and Evaluation of Graduate Education (CAPES, Finance Code 001). The authors would also like to thank the Goiás State Research Foundation (FAPEG, grant no. 2017.10.267000.513) and the Brazilian National Council for Scientific and Technological Development (CNPq, grant no. 552118/2011-7) for financing this research.

REFERENCES

- [1] Q. Deng, W.-J. Yi, and F.-J. Tang, "Effect of coarse aggregate size on shear behavior of beams without shear reinforcement," *ACI Struct. J.*, vol. 114, no. 5, pp. 1131–1142, 2017, <http://dx.doi.org/10.14359/51689720>.
- [2] E. Sells, J. J. Myers, and J. S. Volz, "Aggregate interlock push-off test results of Self-Consolidating Concrete (SCC) for use in infrastructure element," in *Proc. ISEC 2013 - 7th Int. Struct. Eng. Constr. Conf. New Dev. Struct. Eng. Constr.*, 2013, pp. 917–922, <http://dx.doi.org/10.3850/978-981-07-5354-2-St-194-552>.
- [3] D. L. Araújo, F. A. Lobo, and B. G. Martins, "A shear stress-slip relationship in steel fibre-reinforced concrete obtained from push-off testing," *Constr. Build. Mater.*, vol. 293, pp. 123435, 2021, <http://dx.doi.org/10.1016/j.conbuildmat.2021.123435>.
- [4] S. Lee, J.-Y. Cho, and F. J. Vecchio, "Analysis of steel fiber-reinforced concrete elements subjected to shear," *ACI Struct. J.*, vol. 113, no. 2, pp. 275–285, 2016., <http://dx.doi.org/10.14359/51688474>.

- [5] D. L. Araújo, L. C. Carmo, F. G. T. Nunes, and R. D. Toledo Filho, "Modelagem computacional de vigas de concreto armado reforçado com fibras de aço submetidas a cisalhamento," *Rev. IBRACON Estrut. Mater.*, vol. 3, no. 1, pp. 68–94, 2010., <http://dx.doi.org/10.1590/S1983-41952010000100005>.
- [6] J. C. Walraven, *Aggregate Interlock: a Theoretical and Experimental Analysis*. Delft Univ. Technol., 1980. Accessed: Sep. 18, 2022. [Online]. Available: <https://repository.tudelft.nl/islandora/object/uuid:c33a2890-f9c1-4176-929e-6988f0f23640/datastream/OBJ/download>
- [7] J. C. Walraven and H. W. Reinhardt, "Theory and experiments on the mechanical behaviour of cracks in plain and reinforced concrete subjected to shear loading," *Heron*, vol. 26, no. 1A, pp. 1–68, 1981.
- [8] P. G. Gambarova and C. Karakoc, "A new approach to the analysis of the confinement role in regularly cracked concrete elements," in *H - Struct. Eng. Prestressed Reac. Pressure Vessels Other Struct. H5 - Failure, Fracture Propag. Ductility SMiRT 7*, 1983, pp. 251–261.
- [9] B. Li, K. Maekawa, and H. Okamura, "Contact density model for stress transfer across cracks in concrete," *J. Fac. Eng. Univ. Tokyo*, vol. XL, no. 1, pp. 9–52, 1989.
- [10] A. T. Slobbe, M. A. N. Hendriks, and J. G. Rots, "Sequentially linear analysis of shear critical reinforced concrete beams without shear reinforcement," *Finite Elem. Anal. Des.*, vol. 50, pp. 108–124, 2012, <http://dx.doi.org/10.1016/j.finel.2011.09.002>.
- [11] J. A. O. Barros, H. Baghi, S. J. E. Dias, and A. Ventura-Gouveia, "A FEM-based model to predict the behaviour of RC beams shear strengthened according to the NSM technique," *Eng. Struct.*, vol. 56, pp. 1192–1206, 2013, <http://dx.doi.org/10.1016/j.engstruct.2013.06.034>.
- [12] J. Sagaseta, *The Influence of Aggregate Fracture on the Shear Strength of Reinforced Concrete Beams*. Imp. Coll. London, 2008. Accessed: Sep. 18, 2022. [Online]. Available: <https://ibeton.epfl.ch/Pubs/2008/Sagaseta08a.pdf>
- [13] R. Scotta, R. Vitaliani, A. Saetta, E. Oñate, and A. Hanganu, "Scalar damage model with a shear retention factor for the analysis of reinforced concrete structures: theory and validation," *Comput. Struct.*, vol. 79, no. 7, pp. 737–755, 2001, [http://dx.doi.org/10.1016/S0045-7949\(00\)00178-4](http://dx.doi.org/10.1016/S0045-7949(00)00178-4).
- [14] M. A. N. Hendriks, A. de Boer, and B. Belletti, *Guidelines for Nonlinear Finite Element Analysis of Concrete Structures*. Rijkswaterstaat Cent. Infrastruct., Report RTD:1016-1:2017, 2017.
- [15] DIANA FEA, *User's Manual - Material Library - DIANA Release 10.0*, 1st ed. Delft: TNO DIANA BV, 2016.
- [16] J. A. Figueiras, *Ultimate Load Analysis of Anisotropic and Reinforced Concrete Plates and Shells*. Univ. Coll. Swansea, 1983. Accessed: Sep. 18, 2022. [Online]. Available: [https://repositorio-aberto.up.pt/bitstream/10216/11772/2/Texto integral.pdf](https://repositorio-aberto.up.pt/bitstream/10216/11772/2/Texto%20integral.pdf)
- [17] J. G. Rots and J. Blaauwendraad, "Crack models for concrete: discrete or smeared? Fixed, multi-directional or rotating," *Heron*, vol. 34, no. 1, pp. 1–59, 1989.
- [18] V. Červenka, L. Jendele, and J. Červenka, *ATENA Program Documentation - Part 1 - Theory*. Prague: Cervenka Consulting Ltd., 2005.
- [19] A. G. Soto and W. Kaufmann, "Effect of test setups on the shear transfer capacity across cracks in FRC," in *Fibre Reinforced Concrete: Improvements and Innovations* (BEFIB 2020. RILEM Bookseries 30), P. Serna, A. Llano-Torre, J. R. Martí-Vargas and J. Navarro-Gregori, Eds., Cham: Springer, 2021, http://dx.doi.org/10.1007/978-3-030-58482-5_15
- [20] W. Kaufmann, A. Amin, A. Beck, and M. Lee, "Shear transfer across cracks in steel fibre reinforced concrete," *Eng. Struct.*, vol. 186, pp. 508–524, 2019, <http://dx.doi.org/10.1016/j.engstruct.2019.02.027>.
- [21] J. Echegaray-Oviedo, J. Navarro-Gregori, E. Cuenca, and P. Serna, "Modified push-off test for analysing the shear behaviour of concrete cracks," *Strain*, vol. 53, no. 6, pp. 1–17, 2017, <http://dx.doi.org/10.1111/str.12239>.
- [22] DIANA FEA, *User's Manual - iDIANA Release 10.0*, 1st ed. Delft: TNO DIANA BV, 2016.
- [23] fib, *fib Model Code for Concrete Structures 2010*. Berlin: Wilhelm Ernst & Sohn, 2013.
- [24] M. Blomfors, C. G. Berrocal, K. Lundgren, and K. Zandi, "Incorporation of pre-existing cracks in finite element analyses of reinforced concrete beams without transverse reinforcement," *Eng. Struct.*, vol. 229, pp. 111601, 2021, <http://dx.doi.org/10.1016/j.engstruct.2020.111601>.
- [25] American Society for Testing Materials, *Standard Test Method for Flexural Performance of Fiber-Reinforced Concrete (Using Beam With Third-Point Loading)*, ASTM C1609, 2019.
- [26] I. Löfgren, "Fibre-reinforced concrete for industrial construction: a fracture mechanics approach to material testing and structural analysis," Ph.D. dissertation, Dept. Civ. Environ. Eng. Struct. Eng., Chalmers Univ. Technol., Göteborg, Sweden, 2005. Accessed: Sep. 18, 2022. [Online]. Available: <https://publications.lib.chalmers.se/records/fulltext/8627/8627.pdf>
- [27] L. A. G. Bitencourt, O. L. Manzoli, T. N. Bittencourt, and F. J. Vecchio, "Numerical modeling of steel fiber reinforced concrete with a discrete and explicit representation of steel fibers," *Int. J. Solids Struct.*, vol. 159, pp. 171–190, 2019, <http://dx.doi.org/10.1016/j.ijsolstr.2018.09.028>.
- [28] T. L. Resende, D. C. T. Cardoso, and L. C. D. Shehata, "Experimental and theoretical investigation on the stress transfer across cracks due to combined action of steel fibers and aggregate interlock," *Cement Concr. Compos.*, vol. 124, pp. 104239, 2021, <http://dx.doi.org/10.1016/j.cemconcomp.2021.104239>.

- [29] T. Soetens and S. Matthys, "Shear-stress transfer across a crack in steel fibre-reinforced concrete," *Cement Concr. Compos.*, vol. 82, pp. 1–13, 2017, <http://dx.doi.org/10.1016/j.cemconcomp.2017.05.010>.
- [30] L. M. P. Mato, J. A. O. Barros, A. Ventura-Gouveia, and R. A. B. Calçada, "Constitutive model for fibre reinforced concrete by coupling the fibre and aggregate interlock resisting mechanisms," *Cement Concr. Compos.*, vol. 111, pp. 103618, 2020, <http://dx.doi.org/10.1016/j.cemconcomp.2020.103618>.
- [31] F. Soltanzadeh, J. A. O. Barros, and R. F. C. Santos, "High performance fiber reinforced concrete for the shear reinforcement: experimental and numerical research," *Constr. Build. Mater.*, vol. 77, pp. 94–109, 2015, <http://dx.doi.org/10.1016/j.conbuildmat.2014.12.003>.
- [32] D. L. Araújo, F. G. T. Nunes, R. D. Toledo Fo., and M. A. S. Andrade, "Shear strength of steel fiber-reinforced concrete beams," *Acta Sci. Technol.*, vol. 36, no. 3, pp. 389–397, 2014., <http://dx.doi.org/10.4025/actascitechnol.v36i3.19005>.
- [33] S. L. G. Garcia, *Taxa de armadura transversal mínima em vigas de concreto armado*. Univ. Fed. Rio de Janeiro, 2002.
- [34] F. Cavagnis, M. F. Ruiz, and A. Muttoni, "Shear failures in reinforced concrete members without transverse reinforcement: An analysis of the critical shear crack development on the basis of test results," *Eng. Struct.*, vol. 103, pp. 157–173, 2015., <http://dx.doi.org/10.1016/j.engstruct.2015.09.015>.
- [35] J. K. Wight and J. G. Macgregor, *Reinforced Concrete: Mechanics and Design*, 6th ed. Prentice Hall, 2011.
- [36] J. G. Rots, *Computational Modeling of Concrete Fracture*. Delft Univ. Technol., 1988. Accessed: Sep. 18, 2022. [Online]. Available: <https://repository.tudelft.nl/islandora/object/uuid%3A06985d0d-1230-4a08-924a-2553a171f08f>

Author contributions: DLA: supervision, project administration, funding acquisition, methodology, formal analysis, writing. CRSF: methodology, formal analysis, investigation. FAL: methodology, investigation.

Editors: Leandro Trautwein, Mauro Real, Mario Pimentel.